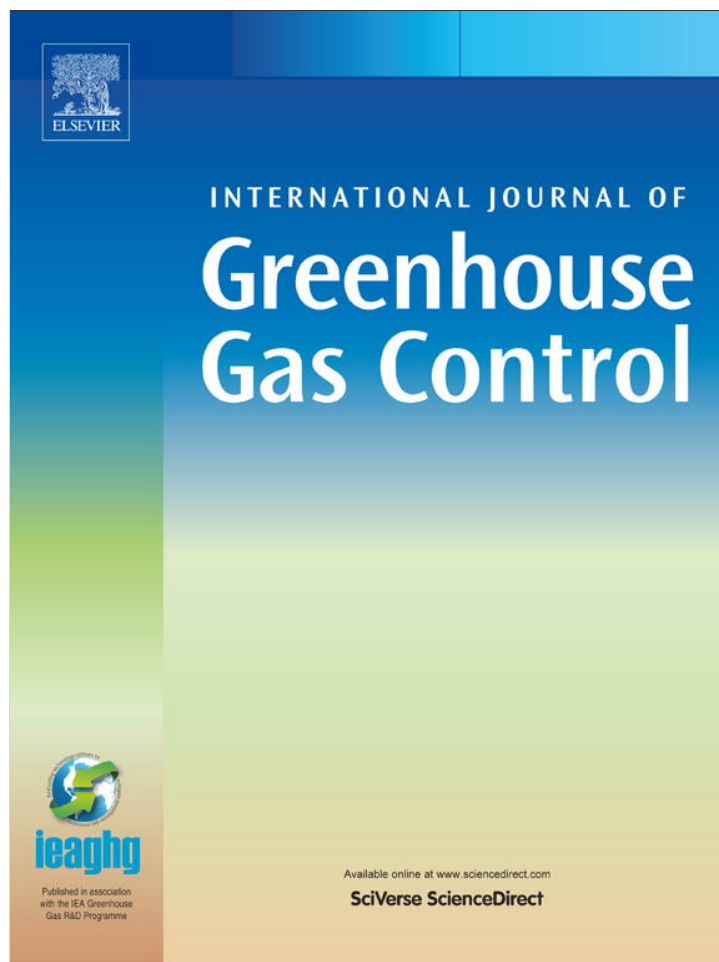


Provided for non-commercial research and education use.
Not for reproduction, distribution or commercial use.



(This is a sample cover image for this issue. The actual cover is not yet available at this time.)

This article appeared in a journal published by Elsevier. The attached copy is furnished to the author for internal non-commercial research and education use, including for instruction at the authors institution and sharing with colleagues.

Other uses, including reproduction and distribution, or selling or licensing copies, or posting to personal, institutional or third party websites are prohibited.

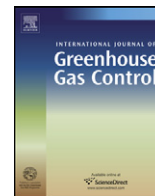
In most cases authors are permitted to post their version of the article (e.g. in Word or Tex form) to their personal website or institutional repository. Authors requiring further information regarding Elsevier's archiving and manuscript policies are encouraged to visit:

<http://www.elsevier.com/copyright>



Contents lists available at SciVerse ScienceDirect

International Journal of Greenhouse Gas Control

journal homepage: www.elsevier.com/locate/ijggcAerial detection of a simulated CO₂ leak from a geologic sequestration site using hyperspectral imageryG.J. Bellante^{a,*}, S.L. Powell^b, R.L. Lawrence^b, K.S. Repasky^c, T.A.O. Dougher^d^a Department of Land Resources and Environmental Sciences, Montana State University, P.O. Box 173120, Bozeman, MT 59717, USA^b Department of Land Resources and Environmental Sciences, Montana State University, United States^c Department of Electrical and Computer Engineering, Montana State University, United States^d Department of Plant Sciences and Plant Pathology, Montana State University, United States

ARTICLE INFO

Article history:

Received 31 July 2012

Received in revised form

27 November 2012

Accepted 28 November 2012

Keywords:

Geologic carbon sequestration

Hyperspectral

Monitoring

Aerial imaging

CO₂ leak detection

Plant stress

ABSTRACT

Airborne remote sensing has been proposed as a potential large-area monitoring tool for geologic carbon sequestration (GCS) sites. Elevated soil CO₂ levels from an underground CO₂ leak could induce a plant stress response that is spectrally discernible from the air. A controlled subsurface CO₂ release experiment was conducted during the growing season at the outdoor Zero Emissions Research and Technology (ZERT) center to simulate a CO₂ leak scenario. Simultaneously, aerial imagery was collected to obtain a time series used to identify and characterize the simulated CO₂ leak prior to, during, and after the three week CO₂ release. A theoretical framework was developed for analytical strategies that could be implemented to detect a CO₂ leak using aerial hyperspectral imagery with minimal *a priori* knowledge of when and where a surface leak is going to occur. Areas of inferred CO₂ stressed vegetation were identified using an unsupervised clustering algorithm. The spectral signatures of this vegetation informed the development of a red edge index (REI) used to quantify the CO₂ stress signal and chart vegetation health trajectories over the course of the CO₂ release experiment. REI was found to be significantly lower (Welch's *p*-value < 0.001) in CO₂ stressed vegetation as compared to healthy vegetation. Furthermore, maximum differences in REI (REI_{healthy vegetation} – REI_{CO₂ stressed vegetation}) were observed at the height of the CO₂ release followed by a subsequent decrease in differences once CO₂ injection ceased. These results suggest that there was a cumulative vegetation stress response followed by a possible vegetation recovery and that aerial hyperspectral imaging may be a plausible method for detecting CO₂ leaks from GCS sites.

© 2012 Elsevier Ltd. All rights reserved.

1. Introduction

1.1. Geologic carbon sequestration

Global surface temperature increased $0.74 \pm 0.18^\circ\text{C}$ from 1906 to 2005 (IPCC AR4 2007). Atmospheric carbon dioxide (CO₂) concentration has risen to over 380 ppm from the pre-industrial level of 280 ppm—the highest level in over 400,000 years (Cuffey and Vimeux, 2001; Monnin et al., 2001; Petit et al., 1999; Seigenthaler et al., 2005). The National Carbon Sequestration Database and Geographic Information System (NATCARB) estimates annual point source emissions to be over 3.8 gigatonnes (Gt) CO₂ for North America (NETL, 2007). North American basalts, deep saline formations, underground coal seams, and depleted oil wells are geologic regions

that are potential storage sites with an estimated total capacity of over 3500 GtCO₂ (NETL, 2008; IPCC, 2005; LBNL, 2000; Mingzhe et al., 2006; Xu, 2004). Currently, there are four industrial-scale geologic carbon sequestration (GCS) projects in operation worldwide: (1) the Salah gas field in Algeria (Rutqvist et al., 2010); (2) the subsea Sleipner project in the North Sea (Korbol and Kaddour, 1995); (3) the Weyburn oil field in Saskatchewan, Canada (Whittaker, 2004); and (4) the subsea Snøhvit gas field in the Norwegian Sea (Maldal and Tappel, 2004). Each of these sites is storing approximately 0.001 GtCO₂/year in enhanced coal bed methane or oil recovery efforts.

Safe and efficient GCS must effectively store large amounts of CO₂ underground for extensive periods of time with minimal surface leakage. It has been proposed that a leakage rate of $\leq 0.01\%$ total CO₂ stored per year would be an appropriate performance requirement to ensure the efficacy of GCS (Benson et al., 2005). Sources of CO₂ leakage from a sequestration site is likely to be confined to improperly sealed well bores, geologic faults, or fractures in the otherwise impermeable cap rock (Benson et al., 2005; Cortis et al., 2008; Knauss et al., 2005; LBNL, 2000; IPCC, 2005; Oldenburg et al., 2009; Pruess, 2008; Wilson et al., 2007).

* Corresponding author.

E-mail addresses: gabriel.bellante@gmail.com (G.J. Bellante), spowell@montana.edu (S.L. Powell), rickl@montana.edu (R.L. Lawrence), repasky@ece.montana.edu (K.S. Repasky), tracyaod@montana.edu (T.A.O. Dougher).

The exact location of a CO₂ surface leak may be unknown to land managers of a GCS site, even though the locations of existing wells and faults will presumably be known. The Department of Energy's (DOE) Regional Carbon Sequestration Partnerships have identified numerous geologic formations as potential GCS sites. These areas are very large and some cover hundreds of square kilometers. There are numerous methods that a CO₂ leak from a GCS site could be detected, however, most are costly, time consuming and resource intensive (Spangler et al., 2009; Strazisar et al., 2009). Ground-based methods could only monitor small areas for CO₂ leakage without an impractical amount of labor resources and equipment. Aerial remote sensing has piqued the interests of managers and researchers because of its potential as a relatively low-cost, practical monitoring tool with large-area coverage capabilities. This study investigated the viability of using airborne hyperspectral remote sensing to detect CO₂ leaks by analyzing imagery collected over a controlled experimental release site.

1.2. Hyperspectral remote sensing for GCS monitoring

Vegetation covers a significant portion of the Earth's land surface and is likely to be the predominant land cover at GCS sites, therefore, it has been postulated that remote sensing could indirectly identify subsurface CO₂ leaks through the detection of plant stress caused by elevated soil CO₂ (Bateson et al., 2008; Keith et al., 2009). Remote sensing has been used to assess plant stress in a wide range of real world applications. Hyperspectral data have been used in particular because of their wealth of continuous spectral information that is collected in many narrow wavelengths throughout the visible and near infrared portion of the electromagnetic (EM) spectrum to derive spectral signatures to differentiate and characterize vegetation (Goetz et al., 1985). Plant reflectance and absorption features that relate to biochemical processes found within narrow band spectra of hyperspectral data can be diagnostic of plant health. These spectral characteristics otherwise could be masked out by conventional, broad-band multispectral remote sensing systems (Lillesand et al., 2008).

1.3. The red edge

Plant stress detection evaluates spectral data in regions that are either sensitive to plant photosynthetic efficiency by detecting changes in absorption and reflectance determined by plant pigment levels or through the detection of changes to physical plant structure. The most commonly studied spectral region to detect plant stress occurs on the boundary of the visible red and near infrared portion of the EM spectrum, termed the "red edge" (~700–750 nm). The red edge is a reflectance pattern in plant spectra associated with heavy *chlorophyll a* and *b* absorption in the visible light wavelengths (400–700 nm), and high reflectance in the near infrared (750–900 nm) due to the spongy leaf mesophyll (Carter and Knapp, 2001; Smith et al., 1997; Zarco-Tejada et al., 2000). Plant stress is known to degrade chlorophyll pigment absorption, increasing the reflectance of photosynthetically active radiation in the visible region of the EM spectrum. Analysis of the red edge can detect plant stress by tracking changes in peak and trough reflectance or changes in the slope derivatives. Narrow band red edge spectral indices, in the form of ratios and derivatives, have been used repeatedly as proxy measure of stress in plants (Buschmann and Nagel, 1993; Carter and Knapp, 2001; Carter and Miller, 1994; Demetriades-Shah et al., 1990; Gitelson and Merzlyak, 1996, 1997; Smith et al., 2004; Strachan et al., 2002; Vogelmann et al., 1993). These hyperspectral indices have the distinct advantage of being more sensitive to smaller, subtle spectral changes than traditional broad band indices, such as the Normalized Difference Vegetation Index (NDVI) or Simple Ratio (SR). Hyperspectral techniques that

use spectral information in the red edge for the proxy measurement of chlorophyll content and plant structure can therefore be used as a measure of photosynthetic activity and stress in plants.

1.4. Plant response to elevated soil CO₂

Elevated soil CO₂ is known to displace oxygen at a plant's roots, thereby inhibiting plant respiration and inducing a stress response (Bergfeld et al., 2006; Maček et al., 2005). Vegetation could act as a "bellwether" for CO₂ leaks at a GCS site if plants exhibit a spectral stress signature in response to elevated soil CO₂. The direct detection of a CO₂ leak by discerning changes in soil CO₂ flux or soil CO₂ concentration within the range of natural background soil CO₂ variability is difficult (Lewicki et al., 2006, 2007), however, the indirect identification of CO₂ leaks through the remote detection of plant stress could be an alternative method. Hyperspectral plant signatures obtained by a ground-based field spectrometer were used to assess plant stress caused by elevated soil CO₂ and detected a plant stress response up to 7.5 m away from a buried release pipe (Male et al., 2010). The most distinguishable plant stress signatures, however, were achieved from plants occurring within a horizontal distance of 2.5 m from a buried CO₂ release pipe (Keith et al., 2009; Male et al., 2010). Another study, investigating the effects of a subsurface natural gas leak, showed that plants within a horizontal distance of 0.5 m from the buried leak source exhibited clear signs of stress due to displaced oxygen at the plants' root zone (Noomen et al., 2008).

Vegetation stress responses to oxygen depleted soil have been expressed as increased reflectance in the visible red and decreased reflectance in near infrared of the red edge (Keith et al., 2009; Male et al., 2010; Noomen et al., 2008; Noomen and Skidmore, 2009). The red edge has also been used in the detection of vegetation stress before it is visible to the human eye. A 5–10 nm shift of the red edge towards shorter wavelengths (called the "blue shift") has been observed and was associated with pre-visual plant stress detection (Carter, 1993; Carter and Miller, 1994; Rock et al., 1988). Pre-visual stress detection has implications for GCS site monitoring, because it could allow for the early identification of CO₂ leaks with hyperspectral remote sensing.

1.5. Airborne hyperspectral imaging for plant stress detection

Leaf and canopy-level remote sensing studies have successfully detected plant stress caused by elevated soil CO₂ conditions using high spatial resolution data obtained on the ground (Keith et al., 2009; Noomen and Skidmore, 2009; Rouse et al., 2010). There have been fewer studies using imagery collected from airborne platforms to specifically detect plant stress (Bateson et al., 2008). Scaling up from ground based to aerial remote sensing can confound the process of detecting plant stress due to changes in the illumination characteristics of a scene, the complexity of vegetation structure, and a coarser spatial resolution (Knipling, 1970). Leaf-level investigations detect reflectance in the near infrared that is determined by the scattering of light energy within the airy, palisade mesophyll layer within plant leaves. Aerial investigations in contrast, detect reflectance in the near infrared that is sensitive to a wider variety of factors, including vegetation stress, shadowing caused by canopy geometry, leaf area index, plant phenology, and the influence of background reflectance of mixed pixels (e.g., soil and understory vegetation). These additional environmental variables, coupled with imaging geometry, make it difficult to separate the physiological plant stress signal of interest from other spectral influencing phenomena (Knipling, 1970). Airborne hyperspectral remote sensing studies, however, have demonstrated that it is possible to detect vegetation stress at the canopy and subcanopy level (Lawrence and Labus, 2003; Sampson et al., 2003).

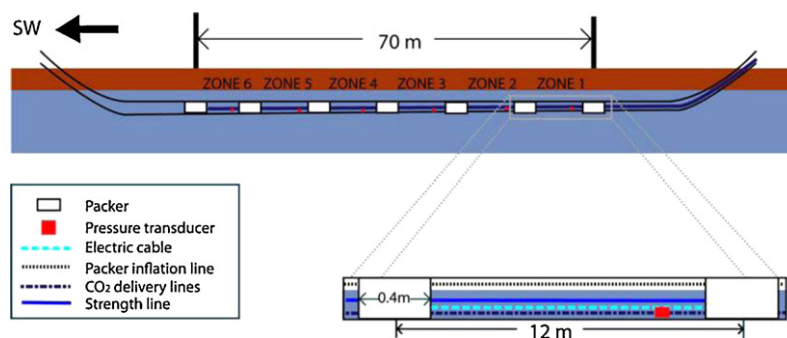


Fig. 1. A cross-section of the buried release pipe at ZERT (Spangler et al., 2009). Zones 1–3 were injected with CO₂ at a rate of 0.2 ton/day (=34.8 kg/day) from June 3, 13:20 to June 24, 14:25 for the June, 2010 release experiment.

A single hyperspectral aerial image of vegetation over a shallow CO₂ release experiment showed that vegetation exhibited a stress response to elevated soil CO₂ (Male et al., 2010). This vegetation, however, was exposed to high levels of soil CO₂ for 27 days and was visibly stressed compared to surrounding vegetation. A single date classification of extremely stressed vegetation due to prolonged exposure to elevated soil CO₂ leaves questions about the efficacy of hyperspectral monitoring and the extent that a CO₂ leak can be detected from an airplane unresolved.

1.6. Research objectives

Several years of research has been devoted to investigating potential GCS monitoring techniques, and no single method has clearly demonstrated that it can meet the monitoring demands of a real-world GCS site. CO₂ leak detection will most likely employ several techniques integrated into a single monitoring system to provide the spatiotemporal accuracy required for adequate surveillance. Land GCS (as opposed to submarine GCS) might encompass a large area that requires a monitoring method with nearly instantaneous data acquisition and large spatial coverage capabilities. We conducted a 2010 aerial imaging campaign with a hyperspectral imager (Resonon Inc.) mounted to a small aircraft to construct a time series of images over a controlled shallow CO₂ release experiment to quantify and characterize the spectral changes to overlying vegetation in response to elevated soil CO₂.

An unsupervised classification was performed to test if locations of known CO₂ leakage could be spectrally identified using the Iterative Self-Organizing Data Analysis Techniques Algorithm (ISODATA). Subsequently, we extracted spectral information from the pixel clusters centrally located over regions known to leak CO₂ at the surface during injection experiments to develop a new narrow band index that was sensitive to the CO₂ stress signal and could be used to compare pixel cluster index trajectories for the time series imagery. The use of an index has the distinct advantages of removing radiometric variability (i.e., weather and atmospheric differences) between imaging dates, as well as simplifying the complex high dimensionality of hyperspectral data for analytical purposes. The narrow band spectral index was then used to analyze the spectral trajectories as a function of distance from the leak source through time in order to develop a method that could be emulated to detect a CO₂ leak around a known area of weakness, such as a well bore or geologic fault.

The goal of these analyses was to provide insight into the feasibility of indirectly identifying CO₂ leaks from GCS sites via the detection of plant stress with airborne hyperspectral imaging by elucidating the timing of CO₂ stress signal detection. Additionally, these analyses are potential remote sensing monitoring strategies that could be deployed in a real-world GCS management framework.

2. Materials and methods

2.1. The experimental CO₂ release site

The Zero Emissions Research and Technology (ZERT) site is a controlled CO₂ release facility located in a 12-ha agricultural field, on the western edge of Montana State University (MSU) in Bozeman, MT (45°39'N, 111°04'W) at an elevation of 1495 m. The ZERT site is characterized by a buried horizontal release pipe that was developed to simulate a longitudinal CO₂ leak source, such as a geologic fault or a weakness in a geologic capstone atop a subsurface reservoir, in order to study potential monitoring tools for GCS technology. The site is on a relatively flat alluvial plain that consists of thick sandy gravel deposits overtopped by several meters of silts, clays, and topsoil (Mokwa, 2006). The buried release pipe is 98 m long with an inner diameter of 10.16 cm and is oriented 45° east of true north. The central 70 m of the pipe is perforated to seep CO₂ during injection. A series of packers were placed within the release pipe to assist in dispersing the gas evenly along the slotted portions of the release pipe (Fig. 1). The pipe was buried using a horizontal drilling technique that minimized disturbance to the surface environment, however, the pipe installation was deflected from a perfectly straight path because of cobble in the gravel layer underground. The surface vegetation is primarily composed of a variety of perennial and annual grasses, alfalfa, dandelion, and thistle.

2.2. Patterns of CO₂ movement from a buried release source

Release experiments at the ZERT site have simulated various GCS leak scenarios to investigate different monitoring tools for quantification and characterization of CO₂ leaks since 2006 (Lewicki et al., 2006, 2007, 2010; Male et al., 2010; Oldenburg et al., 2010; Rouse et al., 2010; Spangler et al., 2009; Strazisar et al., 2009). Research at ZERT has demonstrated that CO₂ injected into the buried release pipe tends to aggregate into local "hot spots" at the surface (Lewicki et al., 2007, 2010; Oldenburg et al., 2010). It is theorized that this pattern of movement is caused by small changes in elevation of the release pipe due to immovable cobble in the subsurface soil and due to soil permeability above the pipe. CO₂ is thought to move from areas of lower to higher elevation within the pipe until the CO₂ is forced upwards by the inserted pipe packers. The CO₂ then follows a path of least resistance to the surface. The CO₂ hotspots have been mapped by accumulation flux chambers (Lewicki et al., 2007, 2010; Spangler et al., 2009) and have been detected spectrally (Keith et al., 2009; Male et al., 2010). The original intent of the release experiments was to have a uniform pattern of release, however, the patchy nature of the surface CO₂ might more closely mimic the conditions of real-world GCS sites where faults or wellbores would mostly be sealed and escaped CO₂ would follow discrete pathways (Lewicki et al., 2007).

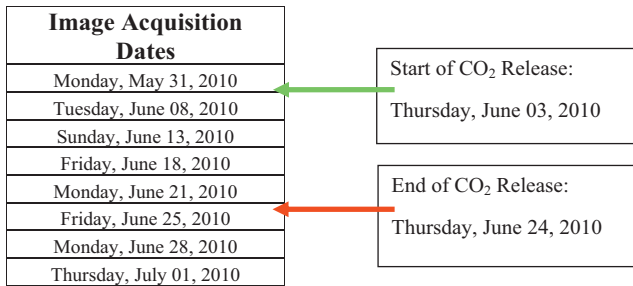


Fig. 2. Image acquisition dates.

Previous and subsequent CO₂ flux maps have shown that the CO₂ hotspots tend to be centered directly over the release pipe and remain relatively unchanged with respect to size and location (Lewicki et al., 2007, 2010; Spangler et al., 2009). We assumed, therefore, that these CO₂ flux maps could be used as reference for the 2010 aerial imaging campaign given that no ground data were collected during the June CO₂ release in order to minimize surface disturbance that could bias our analysis. The CO₂ hotspots originated above the pipe packers with the injected CO₂ radiating outward from the center to form areas of pooled CO₂ that are 2–5-m in diameter.

2.3. 2010 Aerial imaging campaign

The three-week CO₂ injection experiment commenced on June 3, 2010 at 1320 h. CO₂ was injected at a rate of 0.2 ton/day (=200 kg/day) into zones 1, 2, and 3 in order to mimic an annual seepage rate less than the 0.01% CO₂ stored per year of a 500 MW power plant which would result in a total storage of 200 megatonnes (Mt) CO₂ over a 50 year period (Fig. 1). This is assuming that the ZERT site is 1% the area of a typical geologic fault and using the performance standard proposed by Benson et al. (2005). Zones 1, 2, and 3 are sections of the perforated release pipe divided by the first four packers placed at 12 m intervals. The CO₂ injection was terminated on June 24, 2010 at 1425 h.

We collected eight aerial images with a Pika II hyperspectral imager (Resonon Inc.) mounted above a viewing hole in the fuselage of an airplane. The airborne imaging commenced over the ZERT site before, during, and after the three week CO₂ release (Fig. 2). Spectral data were collected in 80 bands throughout the visible and near infrared (NIR) wavelengths (424–929 nm), each with a 6.3 nm channel width. The radiometric resolution of the Pika II sensor was 12-bit quantization at 60 frames per second. The spatial resolution was approximately 0.3 m from the airplane platform at an approximate imaging altitude of 600 m above ground level.

The Pika II was connected to a Resonon PCAQ data acquisition flight computer and an Athena Inertial Navigation System (INS) (Fig. 3). The flight computer was programmed with the UTM coordinates of the ZERT site, which indicated to the imager when to begin and end recording. The INS collected spatial reference data using a Wide Area Augmentation System (WAAS) corrected global positioning system (GPS) and an Inertial Measurement Unit (IMU).

Image acquisition protocol considered three major factors that determine image quality: (1) the bidirectional reflectance function (BRDF); (2) clouds and particulate matter interference; and (3) image distortions due to turbulence. Morning image acquisition was preferable, given that afternoon thunderstorms, cloud formation, and wind were common obstacles to obtaining quality images. Morning dew consistently covered vegetation at this location, however, which could dramatically affect the spectral characteristics of the imagery. Imagery was collected, therefore, at approximately 1200 h on each image acquisition day, which allowed the vegetation enough time to dry out and avoided afternoon storm events.

Each image was acquired perpendicular to the CO₂ release pipe with a flight approach bearing of 135° SE of true north. This flight orientation ensured that the sun angle was parallel to the flight path to limit shadowing effects that influence BRDF.

Tropospheric turbulence is known to greatly influence the stability of an aircraft platform. Images can be skewed due to pitch, roll, and yaw of an aircraft, further complicating the geometric correction process of aligning pixels to ground control points. One of the greatest influences of image distortion is due to the roll motion of an airplane (Jensen et al., 2008), therefore, images were collected with a flight orientation that was directly perpendicular to the release pipe to minimize distortions to the linear position of the buried release pipe. The ZERT site was characterized by nearly uniform vegetation cover with few positively identifiable ground points to use for correcting beyond the internal geometric corrections provided by the Athena INS (Fig. 4). 22 tarps, therefore, were placed at 10-m intervals around the 20-m periphery of the pipe and one more was placed 2 m from the southwest end of the pipe to provide additional identifiable ground control points to aid in geometric correction. The inner two vertices of each tarp (towards the pipe), the pipe ends, and the corners of a semi-permanent storage shed and a temporary scaffolding were geolocated using a survey-grade Trimble R8 GPS receiver with RTK (“real-time kinematic”) corrections from the MSU Continuously Operating Reference Station (CORS) to achieve sub-cm accuracy. Several flight passes were made on each image acquisition day to ensure that some cloud shadow-free, full coverage images were obtained for each date. Imagery was collected on May 31, prior to the CO₂ release, to provide a baseline comparison for subsequent imagery of vegetation exposed to elevated soil CO₂. Imagery was also collected after the termination of the CO₂ release on June 25, June 28, and July 1 to investigate the lingering effects of elevated soil CO₂ and the possibility of a vegetation recovery response.

2.4. Data analysis

2.4.1. Image preprocessing

Acquired raw imagery were filtered to select images that were both cloud and shadow free, as well as contained the entire CO₂ release zone. A single image was chosen for each acquisition date for further analysis. Radiometric corrections were performed by focusing the Pika II sensor into a Gooch & Housego OL Series 455, a National Institute of Standards and Technology (NIST) traceable, calibrated light source that utilizes an integrating sphere to obtain reference spectral response information. Spectral data for every pixel from acquired images were then cross-referenced to the ‘radiometric correction cube’ to obtain a multiplier used to correct for the various gain and shutter settings used by the imager on the different image acquisition dates. The resultant spectral data were given in radiance, in units of microflicks (μf).

Images were then geometrically corrected using the Resonon GeoReg processing software for aligning each pixel to geographic longitude and latitude coordinates. The software integrates data collected by the Athena INS for each image, from each flight, to align the imagery with ground coordinates. This process achieved approximately 3-m spatial accuracy. Further geometric correction was performed by referencing a single image (June 25) to the 56 GPS surveyed ground control points. The other images subsequently, were geo-referenced by registering each individual image to the reference image to achieve sub-meter geometric accuracy. All images were corrected using a 1st order polynomial model within ERDAS Imagine using nearest neighbor resampling (Table 1).

Each of the images was cropped using an area of interest (AOI) within the tarp boundary to isolate the north end of the pipe where the CO₂ release occurred. The artificial structures, reference tarps, and northeast pipe end were masked out to produce images that

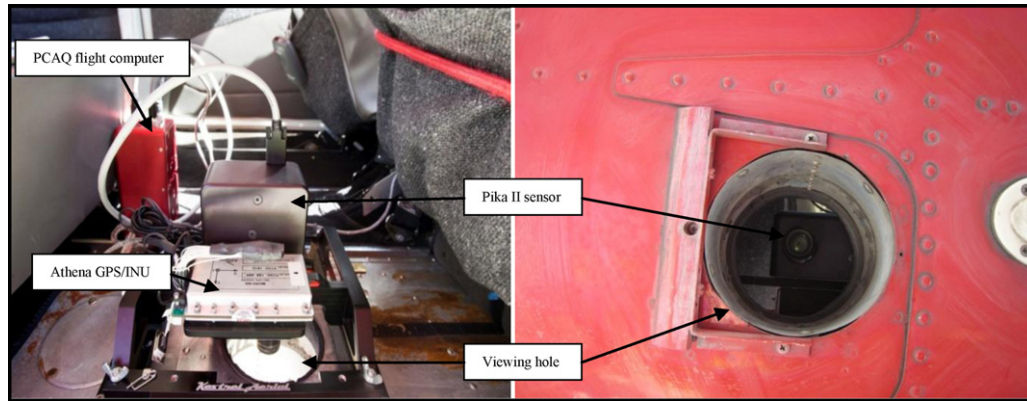


Fig. 3. Sensor setup in the aircraft.

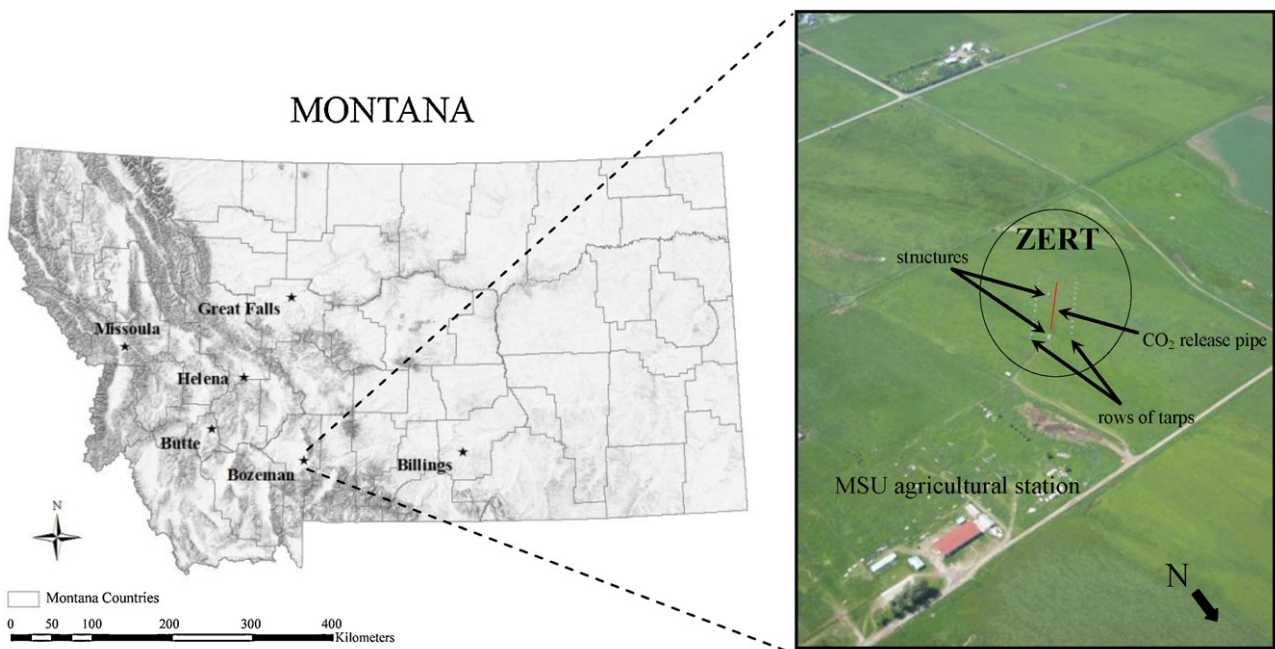


Fig. 4. Location of the study area in Bozeman, MT, and an aerial view of the ZERT site.

Table 1

Summary of each image's spatial resolution and positional error results from the 1st order polynomial geometric correction models using nearest neighbor resampling. GCPs were chosen for accurate identification on both the reference and registered images, therefore, the number of GCPs varied slightly for each date. Each date was resampled using ≥ 50 GCPs.

Reference image			
Date	Spatial Resolution (m)	#of GCPs	Total RMSE (pixels)
June 25	0.34	56	0.2337
Registered images			
Date	Spatial Resolution (m)	# of GCPs	Total RMSE (pixels)
May 31	0.37	50	0.2500
June 8	0.34	54	0.9422
June 13	0.33	55	0.6239
June 18	0.36	51	0.5731
June 21	0.33	51	0.4842
June 28	0.36	52	0.4267
July 1	0.34	50	0.4053

contained only vegetation pixels. Given the high spatial and spectral resolution of hyperspectral data, the subset imagery reduced computer processing time and produced images that were of the same spatial extent for each acquisition date. The resultant eight cropped images contained a rectangular area that was approximately 52 m long by 35 m wide.

2.4.2. Hot spot analysis

This study sought to emulate a process to detect a hypothetical leak from a GCS site when only the location of existing geologic faults and wellbores in the area—the most likely loci for leak occurrence—are known. We performed an unsupervised classification for each image acquisition date to identify regions of CO₂ stressed vegetation.

The unsupervised classification (ERDAS Imagine®) used ISO-DATA with a 0.99 convergence threshold and a maximum of 100 iterations to output 20 vegetation clusters for each image using the 80 band hyperspectral data. Qualitative observation was used to identify “conspicuous” clusters that contained clumps of pixels above the CO₂ release pipe. Alternatively, “inconspicuous” vegetation clusters were labeled as healthy vegetation and not further

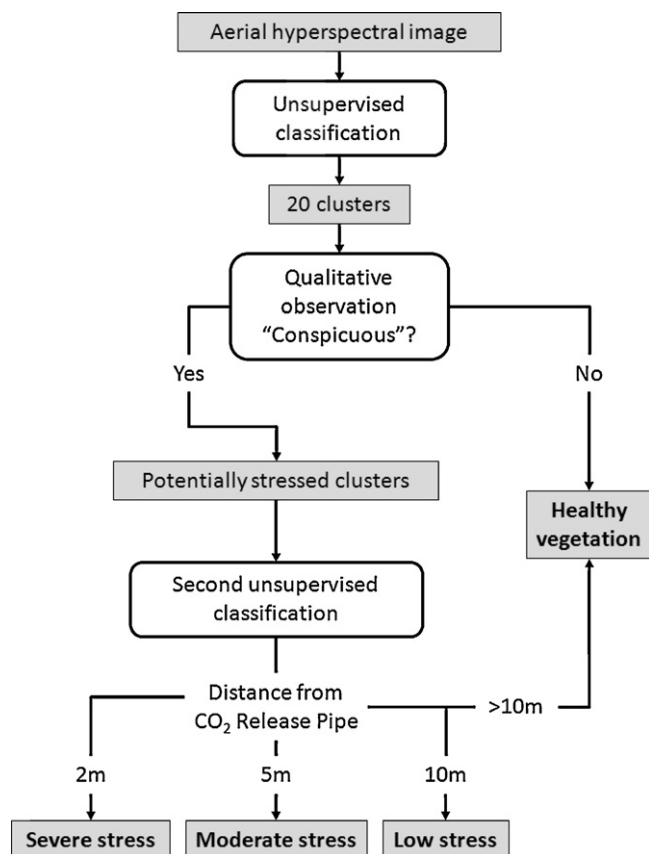


Fig. 5. Flow diagram illustrating the process of class assignment for the unsupervised classification results.

classified. The “conspicuous” clusters were further subdivided by performing a second unsupervised classification to distinguish stressed vegetation from healthy vegetation in convoluted clusters. The second unsupervised classification was performed using the same criteria as the first and resulted in 20 final clusters. Note that each cluster is a grouping of pixels based on spectral similarity, therefore, isolated pixels may exist within a given cluster even if they are not spatially connected. Each of the resultant 20 clusters from the second unsupervised classification was then designated one of four classes using a qualitative coding scheme (Fig. 5).

Previous flux maps at ZERT (Lewicki et al., 2007, 2010; Spangler et al., 2009) have shown that the CO₂ tends to pool in “hot spots”, concentrated areas located above the packers that were placed in the release pipe to create stratified release zones. It has also been shown that the injected CO₂ does not migrate outside of a 10-m radius from the CO₂ release pipe. Considering this, pixel clusters for each date were coded as the following vegetation classes: severe stress (red) if 100% of the cluster pixels occurred within 2-m of the release pipe; moderate stress (orange) if 100% of the cluster pixels were within 5-m from the pipe; low stress (yellow) if 100% of the cluster pixels were within 10-m of the release pipe; and healthy (not coded) if any of the cluster pixels were further than 10-m away from the release pipe. Spectral information was extracted for all the pixels contained within each of the vegetation stress classes. A companion stratified random subset of healthy vegetation pixels, equal in pixel count to the most severe vegetation stress class coded for that date, within each scene was collected. Spectral information for each of the 80 Pika II bands was then extracted and averaged for each CO₂ stress class and each companion subset of healthy pixels to compare spectral signatures of healthy and CO₂ stressed vegetation for each image. It was assumed that vegetation within

pixel clusters closer to the CO₂ release pipe would exhibit more stress than those clusters that were further away.

A spectral index was developed based on the unsupervised classification results that separated pixel clusters known to be associated with CO₂ leakage and those that were not, to amplify the CO₂ stress signal and to chart plant stress trajectories for the ZERT imaging time series. This index ratioed the peak and trough radiance values of the red edge to create the red edge index (REI), an index sensitive to both chlorophyll absorption in the visible red (the trough) and physical vegetation changes (e.g., leaf area index and canopy geometry) in the near infrared (the peak). The REI, therefore, is a proxy spectral indicator of vegetation stress and allowed for the evolution of the CO₂ stress signal to be evaluated at the ZERT site over the course of the release experiment. The REI for healthy vegetation was expected to be greater than the REI for CO₂ stressed vegetation. The difference in REI (REI_{healthy vegetation} – REI_{CO₂ stressed vegetation}) would be significantly greater than zero (Welch’s *p*-value < 0.05) if elevated soil CO₂ concentrations caused a vegetation stress signal in REI that was statistically distinct from healthy vegetation. Statistical significance is sample size dependent and can be influenced by spatial autocorrelation between pixels that can cause type I error, however. The difference would not be significantly different if the stressed and healthy vegetation were not spectrally distinct and of the same population. Vegetation was expected to exhibit more stress as the CO₂ injection progressed, that is the difference in REI should increase with longer exposure to injected CO₂, and vegetation should not exhibit further stress after the termination of the CO₂ release, that is the difference in REI should stay the same or decrease once the CO₂ injection ceased.

2.4.3. Proximity analysis

Plant spectral response was then examined as a function of distance from the CO₂ release pipe for the image time series acquired over the ZERT site. GCS site managers with *a priori* knowledge of areas susceptible to potential CO₂ leakage could therefore employ this strategy for monitoring around these loci. GPS survey points were used in conjunction with the INS data to correct the images to sub-meter positional accuracy on the ground, however, this was insufficient for tracking changes in individual pixels through time. Variable turbulence during image acquisition flights also caused altitude to be inconsistent resulting in different spatial resolutions for each imaging date (Table 1). The REI that was developed from the hotspot analysis was therefore used to assess vegetation stress levels by comparing pixels that were closer to the CO₂ release pipe with pixels that were further away for each image date by using different radius buffer delineations around zones 1–3 of the buried release pipe (Fig. 6). Mean REI calculated for pixels inside each buffer radius (closer to the CO₂ release source referred to hereinafter as release zone pixels) was compared with the mean REI of all the pixels outside that particular buffer boundary (further away from the CO₂ release source referred to hereinafter as healthy zone pixels). This process was performed for each the 1-m, 2-m, 5-m, and 10-m radius buffers. Spectral trajectories were then developed by charting mean REI through time as a function of distance from the buried release pipe in order to track changes in vegetation stress response to elevated soil CO₂ concentration over the course of the experiment.

3. Results

3.1. Hot spot analysis

The results of the unsupervised classification identified areas of inferred vegetation stress in 7 of the 8 imaging dates (Table 2). June

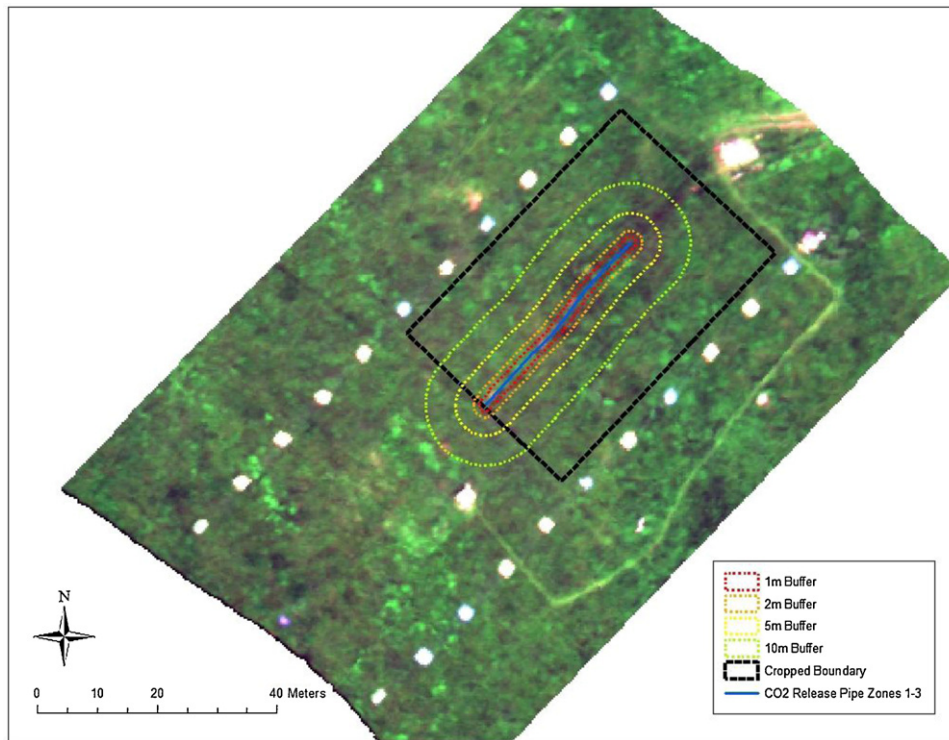


Fig. 6. Study design of the 2010 ZERT aerial imaging campaign. Aerial hyperspectral image displayed in true color with the cropped boundary of vegetation used in both analyses for all image dates along with the different radius buffer boundaries used in the proximity analysis.

8 was the first image collected after the CO₂ release began and on this day—5 days after the initiation of the CO₂ injection—CO₂ stress in vegetation was classified. July 21 was the final imaging day before the CO₂ release was terminated and it contained the highest proportion of clusters (5 of the 20 clusters in the second unsupervised classification) that met the criteria for moderate and severe vegetation stress. The July 21 image also contained the largest total area of inferred vegetation stress (16.33 m²). The CO₂ injection was terminated on June 24. Areas of inferred vegetation stress believed to be caused by elevated soil CO₂ concentrations continued to be classified more than 1 week after the CO₂ injection stopped, although the total area shrank to 6.70 m² (Table 2).

Visual interpretation of the unsupervised classification results showed that the areas first classified as severe vegetation stress in the June 8 image are the same areas that reappear and persist throughout the time series as severe stress in five of the six subsequent images (Fig. 7). These inferred areas of severe vegetation stress generally grew in area and remained consistent in location for the duration of the aerial campaign. There was a high degree

of spatial correlation between the locations of inferred vegetation stress and the centroids of the mapped CO₂ hotspots (regions of high CO₂ flux) derived from CO₂ flux measurements obtained on the ground from a subsequent CO₂ release experiment (Fig. 8).

The mean spectral signatures for each vegetation stress class were compared for each image date and revealed patterns of vegetation spectral response to the CO₂ release over the course of the experiment (Fig. 9). Radiance increased in the visible portion of the EM spectrum for the severely stressed vegetation classes, while the low and moderately stressed vegetation classes exhibited slightly lower radiance values, as compared to healthy vegetation. All of the stress classes do converge and exhibit a similar response in the near infrared. The red edge was not observed to shift towards shorter wavelengths for CO₂ stressed vegetation. Red edge mean peak radiance decreased and mean trough radiance increased for the severe vegetation stress class as compared to the healthy vegetation class. Severe vegetation stress responses within the inflection peak and trough radiance values of the red edge were inversely related, and therefore, were used to develop an index (Fig. 10). The REI was a

Table 2
Number of vegetation stress clusters included within each vegetation stress class and the area (m²) contained therein from the unsupervised classification results in the hot spot analysis.

Vegetation stress classes				
Date	Severe stress class (area in m ²)	Moderate stress class (area in m ²)	Low stress class (area in m ²)	Total # of stress clusters (total area in m ²)
5/31	0(0)	0(0)	0(0)	0(0)
6/08	1(1.73)	1(6.82)	0(0)	2(8.55)
6/13	0(0)	0(0)	1(3.59)	1(3.59)
6/18	1(4.02)	0(0)	0(0)	1(4.02)
6/21	2(3.81)	3(12.52)	0(0)	5(16.33)
6/25	1(4.39)	0(0)	1(6.24)	2(10.63)
6/28	1(3.63)	0(0)	0(0)	1(3.63)
7/01	1(6.70)	0(0)	0(0)	1(6.70)

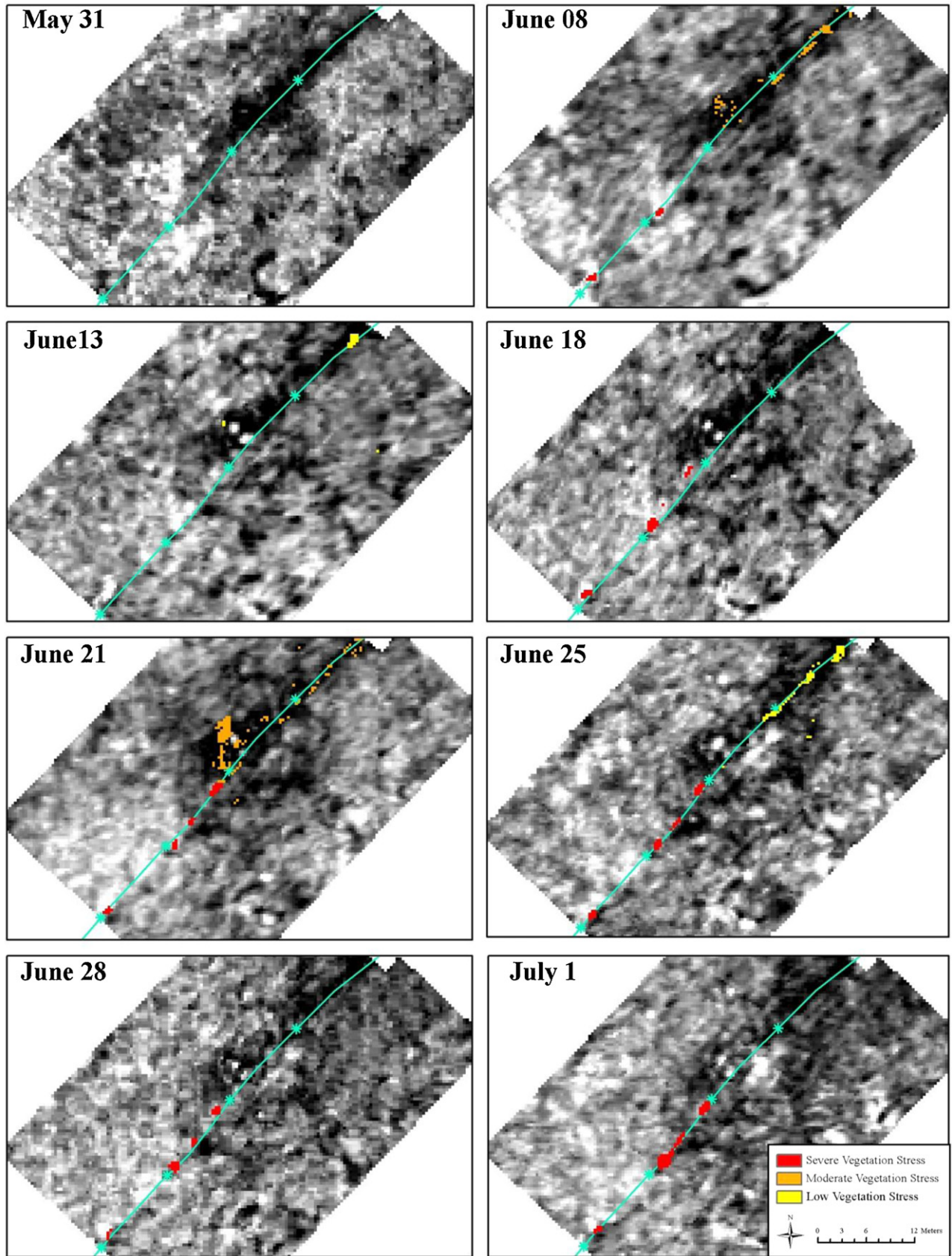


Fig. 7. Unsupervised classification results for ZERT time series. Images are displayed with a green band (band 21: 552 nm) in grayscale.

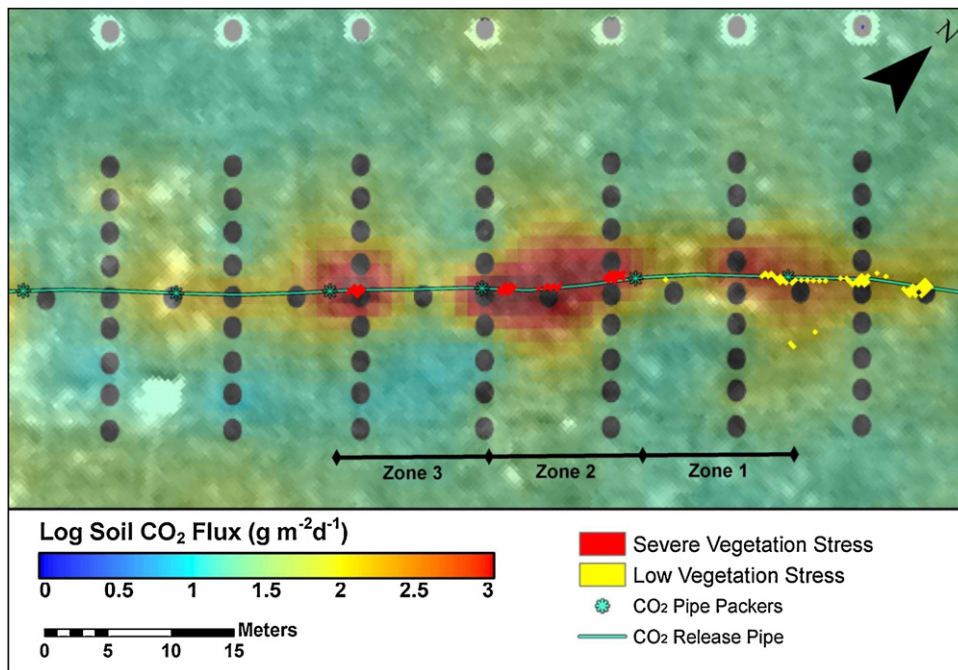


Fig. 8. Map of the classified vegetation stress from the June 25, 2010 unsupervised classification result overlay a CO₂ flux map derived from accumulation chamber ground measurements collected by Jennifer Lewicki of the Lawrence Berkeley National Lab on July 29, 2010 with an estimated leakage discharge of 0.14 t CO₂ d⁻¹.

ratio of the peak narrow-band radiance at 750 nm (Pika II band 52) and the trough narrow-band radiance at 674 nm (Pika II band 40) to amplify the vegetation stress signal believed to be caused by elevated soil CO₂ concentration (Eq. (1)).

$$\begin{aligned} \text{Red Edge Index} &= \frac{\text{radiance}(\text{nir})}{\text{radiance}(\text{red})} = \frac{\text{radiance}(\text{band 52})}{\text{radiance}(\text{band 40})} \\ &= \frac{\text{radiance}(750 \text{ nm})}{\text{radiance}(674 \text{ nm})} \end{aligned} \quad (1)$$

A stress signal was detected after the CO₂ injection began with the difference in REI (REI_{healthy vegetation} – REI_{CO₂ stressed vegetation}) being significantly greater than zero (Welch's *p*-value < 0.001) for all dates that contained a severely stressed vegetation class. The difference in REI increased until the termination of the CO₂ release, after which the difference between the healthy and severely stressed classifications diminished, albeit still spectrally distinguishable (Fig. 11).

3.2. Proximity analysis

The proximity analysis results for each of the different buffers were mostly consistent with our expectations for a vegetation stress response to elevated soil CO₂. The expectation was that the REI should be higher for the healthy zones as compared to their companion release zones, however, this was the case only later in the CO₂ release (Fig. 12). Prior to CO₂ injection, on May 31, all release zone pixels for all buffers (closer to the buried CO₂ release pipe) actually exhibited a greater REI than the healthy zone pixels. REIs of the vegetation pixels contained within the release zone were significantly lower (Welch's *p*-value < 0.001) than those outside at the height of the CO₂ release.

The smaller the fixed radius the faster the rate of divergence in REI, indicating that pixels in closer horizontal proximity to the buried CO₂ release source exhibited more vegetation stress (Fig. 13). The vegetation stress signal believed to be caused by the

CO₂ release diminished as the buffer radius increased in horizontal distance from the buried CO₂ release source. Even though the regression models show linear upward trends of divergence as a function of time, every buffer radius exhibited a drop in REI difference on July 1.

4. Discussion

4.1. Hot spot analysis

The hot spot analysis of the aerial imagery obtained at the ZERT site demonstrated the ability to detect spectral anomalies that were most likely associated with surface plant stress caused by an underground CO₂ leak even when the exact location of surface leakage was not known *a priori*. The locations of the severely stressed vegetation classes corresponded with the centroids of known hot spot locations in previous and subsequent CO₂ release experiments (Lewicki et al., 2007, 2010; Spangler et al., 2009). It is likely that the pattern of CO₂ movement observed at ZERT would mimic the movement of CO₂ leaked from a GCS site because the upward migration of injected CO₂ would follow paths of least resistance and escape through confined areas of weakness given that sequestration sites will be chosen for their geologic integrity (Lewicki et al., 2007).

Analysis of the May 31 image provides a baseline of the pre-release status and overall characterization of the ZERT vegetation before CO₂ injection began. It was important that all subsequent analysis was compared to the initial health of the vegetation above the CO₂ release zones because there was the potential for residual effects from prior CO₂ release experiments that could have influenced vegetation spectral characteristics at the ZERT site. The previous CO₂ release experiment ended in August, 2009. The May 31 image did not contain pixel clusters that qualified for any of the stress classes from the unsupervised classification results because it was obtained prior to the CO₂ release and residual stress was not detected. The June 8 unsupervised classification result discerned severely stressed vegetation at the location of the two major hot

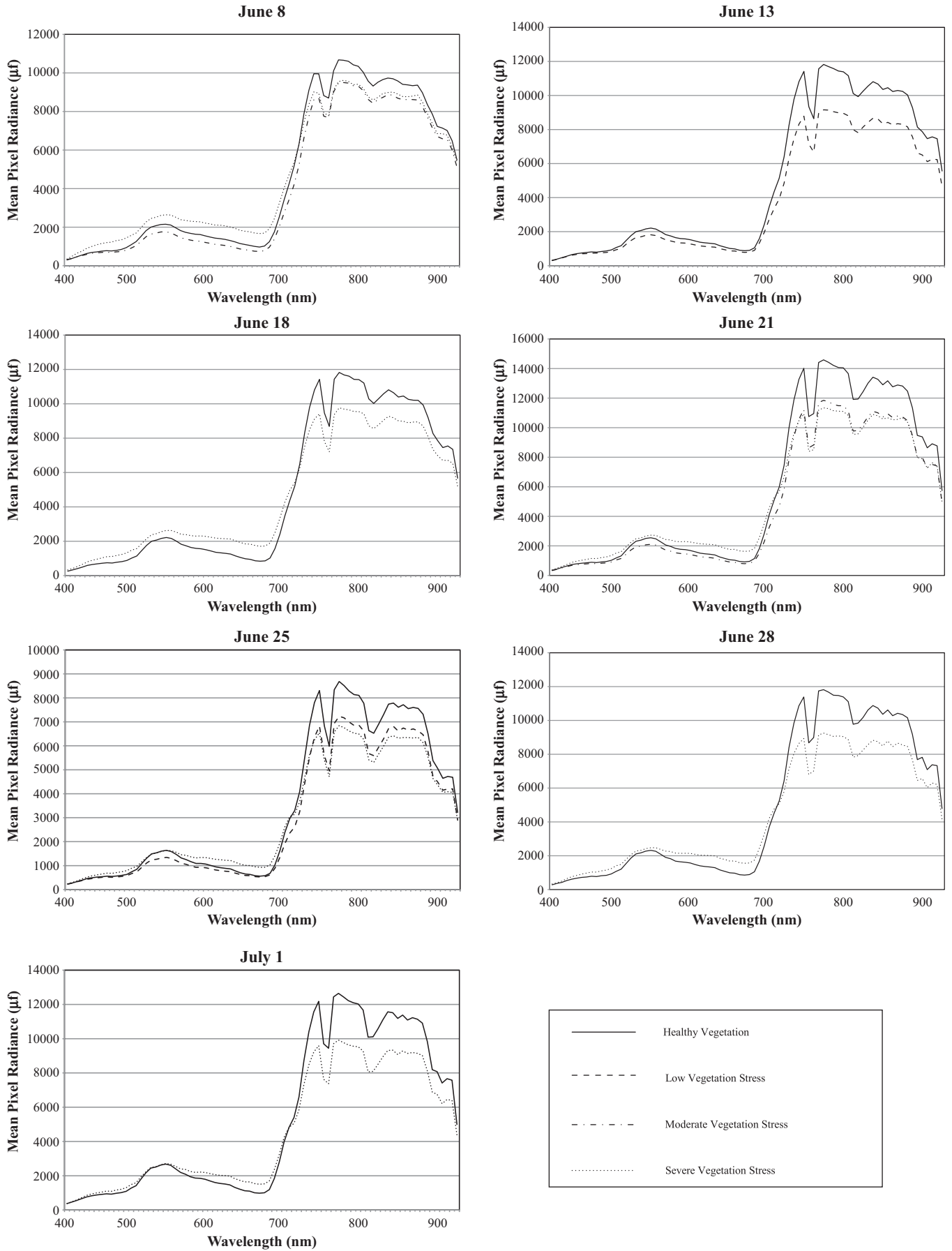


Fig. 9. Spectral signature comparisons for the unsupervised classification time series. The plotted spectral data is the mean radiance (μf) for each vegetation stress class and the randomly selected pixels classified as healthy for each date.

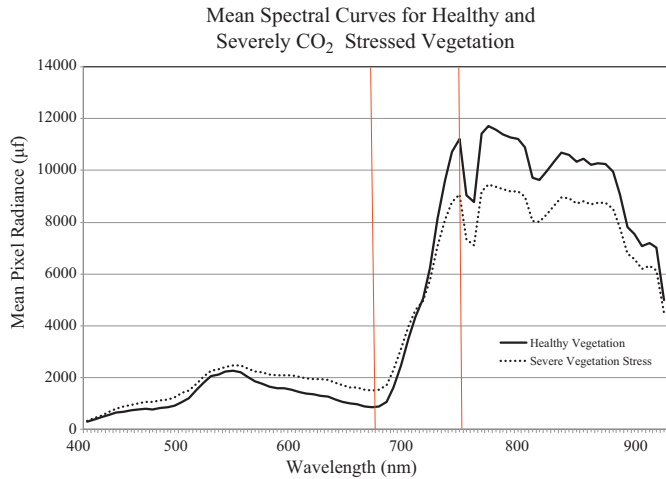


Fig. 10. Mean spectral signatures for all pixels classified as severe vegetation stress and their randomly selected companion healthy pixels for the ZERT time series imagery in mean radiance (μf). The red lines indicate the peak (674 nm) and trough (750 nm) of the red edge, which were used to develop the spectral index (the REI) used as an indicator of vegetation stress caused by elevated soil CO_2 concentrations. (For interpretation of the references to color in this figure legend, the reader is referred to the web version of the article.)

spots that have repeatedly been observed above zones 1 and 2 during other CO_2 release experiments. Although we did not observe a shift in the red edge towards shorter wavelengths for stressed vegetation that has been associated with pre-visual plant stress detection (Carter, 1993; Carter and Miller, 1994; Rock et al., 1988), the accurate identification of these hot spots occurred only five days after the CO_2 injection began. At this time there were no visible changes to the ZERT vegetation as observed from the airplane or on the ground. This was perhaps evidence of pre-visual vegetation stress detection with a hyperspectral imager. Detection of the major hot spots persisted in the subsequent unsupervised classification results. The hot spots increased in size from the time of initial detection, except for the June 13 classification where the hotspots were confused with a small area of vegetation that was located more than 10 m from the release pipe, and therefore, they were not mapped. This vegetation that caused the confusion was potentially stressed by something other than CO_2 , such as human trampling or from deer bedding down at night. Additionally, some

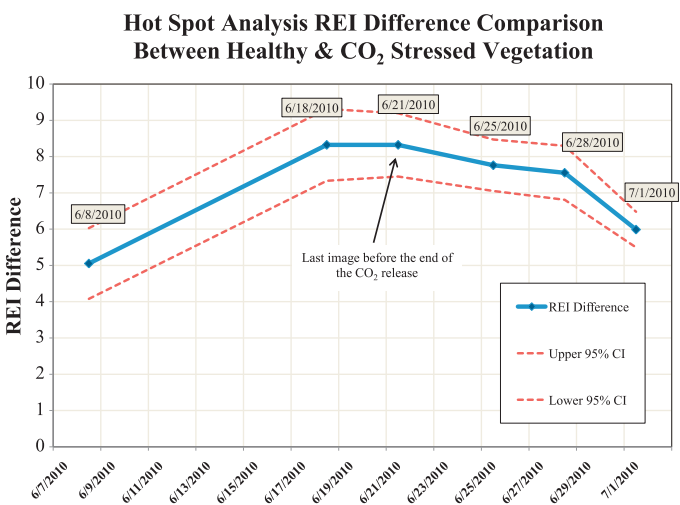


Fig. 11. Difference in REI ($\text{REI}_{\text{healthy vegetation}} - \text{REI}_{\text{CO}_2 \text{ stressed vegetation}}$) between healthy and severely stressed vegetation classes from the unsupervised classification hot spot analysis.

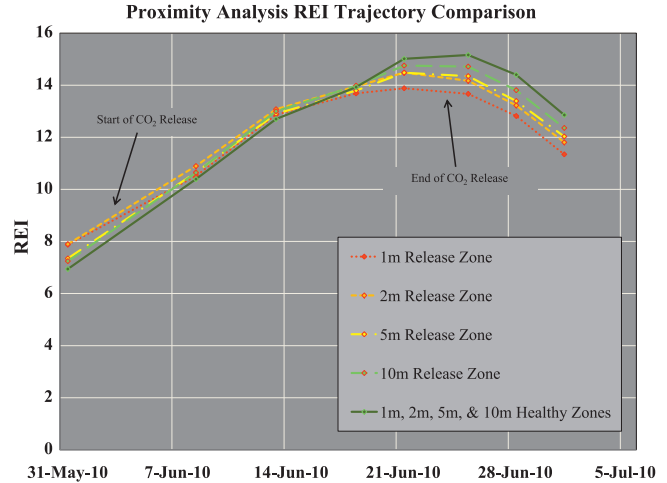


Fig. 12. REI comparison for the different buffer radii around the CO_2 release pipe. Mean REI was calculated for all of the pixels contained within each buffer distance and for all of the pixels outside that particular buffer for each image date. Note, mean REI for each of the healthy zones (pixels outside each of the variable buffer release zones) overlap, indicating spectral similarity in REI.

of the pixels classified as stressed did not correspond with known regions of high CO_2 flux, such as some of the pixels classified as moderate stress on June 21 (Fig. 7). This could be attributed to the detection of false positives and depicts the limitations that exist with the indirect detection of CO_2 leaks.

Aerial imaging geometry, topography, plant phenology, and vegetation stress unrelated to elevated CO_2 concentration in soil would likely confound the process of CO_2 leak detection because of the misidentification of false positives in a monitoring context (Bateson et al., 2008). Although the unsupervised classifications provided a method to identify spectral anomalies associated with areas of high CO_2 flux, a real-world surface CO_2 leak would need to not only elicit a detectable vegetation stress response but would also require ground verification because of the inherent complexity that exists in the natural environment.

Qualitative analysis of the spectral signatures raised questions about the reasons for disparity in spectral response between the different stress classes. Stressed vegetation normally exhibits increased radiance in the visible portion of the spectrum due to suppressed photosynthetic activity (Carter and Knapp, 2001; Smith

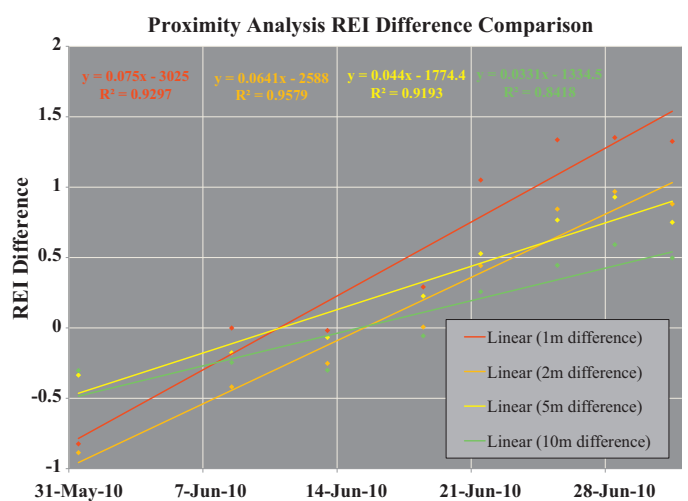


Fig. 13. Fitted linear regression models for the difference in mean REI between the release zones and companion healthy zones for each buffer distance show trends in slope, indicating rates of health divergence.

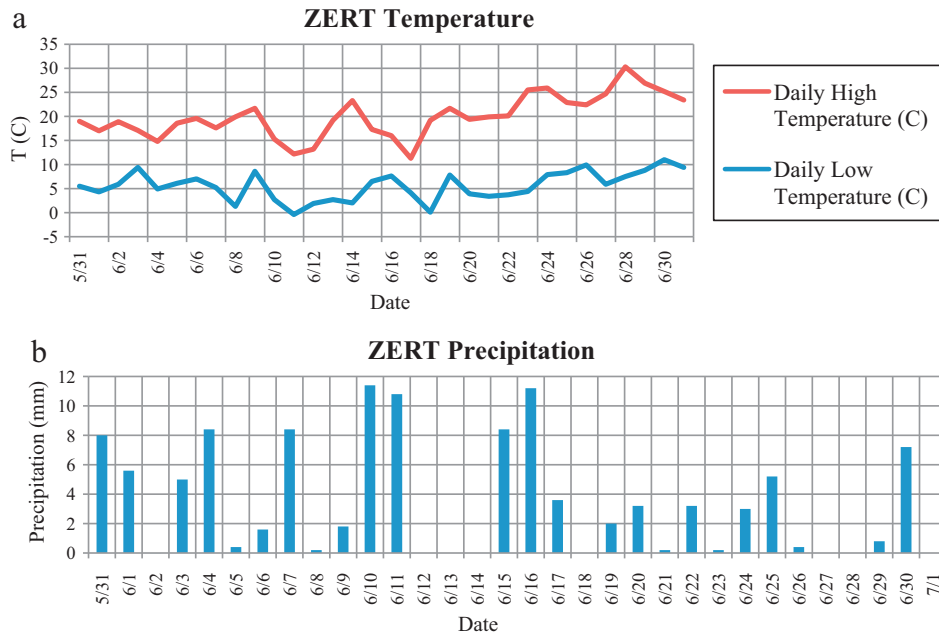


Fig. 14. (a and b) ZERT weather over the course of the 2010 aerial imaging campaign.

et al., 1997; Zarco-Tejada et al., 2000). Low and moderate stress classes, however, exhibited lower radiance values in the visible portion of the spectrum as compared to healthy vegetation, while the severe stressed vegetation expressed increased radiance. Perhaps the low and moderately stressed vegetation experienced a CO₂ fertilization effect from locally high levels of ambient CO₂ located above the CO₂ release pipe. Elevated atmospheric CO₂ has been shown to increase photosynthesis and cause plants to assimilate CO₂ into non-structural organs, such as leaves, which could have caused some of the vegetation above the CO₂ release pipe to increase absorption in the visible spectrum (Ainsworth and Long, 2004). Alternatively, increased visible radiance expressed by the severe stress class could have been attributed to background soil rather than a decrease in photosynthetic activity.

The REI trajectories through the image time series illustrated the initial detection of the CO₂ stress signal on June 8 and the amplification of the CO₂ stress signal as the injection progressed with the hot spots being most discernable after two weeks of elevated soil CO₂ exposure on June 18 and June 21. The REI trajectories also illustrated the subsequent abatement of the CO₂ stress signal in the June 25, June 28, and July 1 images after the termination of the CO₂ injection on June 24, perhaps indicating vegetation recovery. The difference in REI of the randomly selected healthy pixels and the severely stressed pixels for each unsupervised classification result were decreasing with time after the CO₂ injection ceased. This would be consistent with a vegetation recovery, but could be attributed to a synchronous plant senescence event that would cause a disproportionate spectral response in the healthy vegetation pixels. This response would then cause “healthy” pixels to more closely resemble the CO₂ stressed pixels.

4.2. Proximity analysis

The curvilinear time series trend of REI for all of the vegetation pixels demonstrates increasing plant vigor for all pixel groups until June 21, when the REI begins to tail off. This pattern is likely due to both seasonal plant phenological events, as well as responses to local weather. There were only eight rain-free days during the 2010 aerial campaign, and the average daily high temperature at the ZERT site was steadily climbing throughout the course of the

experiment (Fig. 14a and b). Due to the relatively wet weather and increasing ambient temperature, this trend in REI was most likely related to vegetation moisture content as the vegetation at ZERT was drying out by the end of June. Although REI is sensitive to plant vigor as well as plant stress, the stress signal might be isolated by comparing the REI of pixels affected by the CO₂ release to those that were either not affected by the CO₂ release or were further from the release pipe.

The proximity analysis of the different radius buffers surrounding the buried CO₂ release pipe at ZERT provided a method that a GCS site manager could use to examine imaged vegetation pixels surrounding potential point or line sources of leakage, such as a well bore or a geologic fault, for CO₂ stress signals. The REI trajectories for the time series were congruent with a comparatively greater stress response for smaller buffer radii as compared to their companion pixels surrounding the buffers. Meeting the expectation that pixels closer to the CO₂ release pipe were more spectrally distinct from pixels that were further away. Differences in mean REI between the healthy and stressed pixel groups prior to the CO₂ release was negative, which would imply that the release zone pixels were initially ‘healthier’ than the healthy zone pixels (Fig. 12). This difference was most likely attributable to variability in phenological expression and species composition at the ZERT site. The differences in REIs were positive, however, for the 1 m, 2 m, and 5 m buffers beginning June 18, and for the 10 m buffer beginning June 21. More importantly, the differences in REI for the different radii all showed a clear upward linear trend with the smaller radii exhibiting comparatively steeper slopes. This was indicative of a progressively greater rate of divergence in REI between healthy and release zone pixels. Notwithstanding the non-uniformity of the ZERT vegetation structure, these trends are consistent with a vegetation stress response to elevated soil CO₂. The proximity analysis corroborates the results of the hot spot analysis.

The CO₂ stress signal was first detected on June 8, given the immediate upward trend of the differences in REI for all of the different radius buffers. It continued to be registered and increased as the CO₂ injection progressed. All of the different radii exhibited a drop in REI difference between healthy and release zone pixels by July 1, perhaps indicating vegetation recovery after the termination of the CO₂ injection. These results were consistent with

an early remote detection of a CO₂ leak in vegetation that was unmanipulated, in contrast to previous analyses at the ZERT site that characterized CO₂ releases when the vegetation was mechanically mown to uniform height and were evaluated with instruments causing impacts to the surface environment (Male et al., 2010; Spangler et al., 2009).

5. Conclusions

The analysis techniques offered herein present a methodology by which imagery collected with a low-cost aerial hyperspectral monitoring system could be used to inform a focused ground assessment to affirm or refute the detection of a CO₂ leak. This proposed monitoring system would provide broad spatial coverage while minimizing costs and labor requirements. Although our results provide evidence that hyperspectral remote sensing could be a complimentary monitoring tool that may aid in the detection of CO₂ leaks at GCS sites, further study is required to evaluate several key questions. First, both analyses examined REI trajectories, which only utilized 2 narrow spectral channels (674 nm and 750 nm). These bands were deliberately chosen for their sensitivity to the CO₂ stress signal within the red edge based on the unsupervised classification results that utilized information collected in all 80 Pika II bands. Ground monitoring studies at ZERT, however, have demonstrated that by using a multi-spectral imaging system, utilizing broad spectral channels, detection of CO₂ stress in plants is possible (Rouse et al., 2010). Questions remain as to whether or not a broad band, multi-spectral imager could be used to detect CO₂ stress from an aircraft or if a narrow band, 2-channel imager devoted to CO₂ leak detection would suffice for monitoring GCS sites. Higher CO₂ leak detection rates might also have been possible if a method was developed that used all of the spectral information afforded a hyperspectral instrument.

The unsupervised classification distinguished a cluster of vegetation pixels in an area of elevated soil CO₂ on June 8, perhaps providing evidence of early, maybe even pre-visual, stress detection from an airplane, further study is warranted because the vegetation at the ZERT site exhibited signs of a disturbance legacy as a result of repeated CO₂ exposure. Successive release experiments over the past several summers have potentially altered the vegetation community and phenology above the buried release pipe from its original state. It must be assumed that the spectral characteristics of the vegetation impacted by the CO₂ releases are not consistent with respect to the surrounding vegetation through time. The current response of ZERT vegetation to elevated soil CO₂ stress could be confounded if the distribution of vegetation species and/or vegetation density has changed. Also, the semi-automated unsupervised classification process comes with the caveat of false positives, which could diminish the efficiency of this leak detection technique.

The unsupervised clustering algorithm identified regions classified as severely stressed vegetation throughout the release, whereas, low and moderately stressed vegetation classes were infrequently identified. Further spectral analyses of these clusters, therefore, were not performed. It is worth noting that the pixel clusters classified as low and moderate vegetation stress exhibited lower radiance in the visible portion of the EM spectrum (perhaps indicating higher chlorophyll absorption, differences in vegetation, or shadowing effects), while exhibiting lower radiance in the near infrared compared to healthy vegetation. The low and moderately stressed pixels, thus, behaved like healthy pixels in the visible and like severely stressed pixels in the near infrared. This would be problematic for using the REI to identify regions of low and moderate vegetation CO₂ stress and is a danger to using ratio-based

indices because you could get the same index value despite having very different visible and near infrared reflectance for two different spectra. This unexpected result may be due to spatial autocorrelation between the stressed clusters. Alternatively, this result may be evidence of a possible fertilization effect from locally high concentrations of atmospheric CO₂ in the vegetation canopy. The question of how subtle or small a CO₂ leak could be detected still remains unanswered by this study.

Another potential limitation of using remote sensing to indirectly monitor for CO₂ leaks at GCS sites is the influence of seasonality. Imaging must commence when vegetation will exhibit a stress response to elevated soil CO₂ for remote sensing to be a viable monitoring technique. Further investigation is necessary to understand how sensitive plants are to CO₂ stress throughout their growth cycle. This experiment demonstrated that vegetation appears to be sensitive to the CO₂ stress signal during the height of the growing season. Imaging took place when the water table was very high, and during the first couple of weeks over the CO₂ release experiment there was standing water overlying portions of the buried release pipe at ZERT. Standing water could have directly interfered with the spectral data or possibly contributed to vegetation stress and altered the movement of the underground injected CO₂. Knowledge of the spectral influence of vegetation senescence is critical to understanding the limitations of remote sensing of plant stress caused by elevated soil CO₂.

Finally, regarding the sensitivity of vegetation to the CO₂ stress signal, questions remain as to whether or not the CO₂ stress signal is spectrally unique as compared to other plant physiological stressors. For instance, does vegetation that is experiencing stress caused by elevated soil CO₂ look spectrally distinct from trampled vegetation or vegetation experiencing water stress? It will be important to understand whether different sources of physiological plant stress are spectrally discernable in order to properly interpret vegetation stress signals during image analysis. Perhaps the highly dimensional nature of hyperspectral data lends itself to discriminating among different types of vegetation stress.

References

- Ainsworth, E.A., Long, S.P., 2004. What have we learned from 15 years of free-air CO₂ enrichment (FACE)? A meta-analytic review of the responses of photosynthesis, canopy properties and plant production to rising CO₂. *New Phytologist* 165, 351–372.
- Bateson, L., Vellico, M., Beaubien, S.E., Pearce, J.M., Annuziatelli, A., Ciotoli, G., Coren, F., Lombardi, S., Marsh, S., 2008. The application of remote-sensing techniques to monitor CO₂-storage sites for surface leakage: method development and testing at Latera (Italy) where naturally produced CO₂ is leaking to the atmosphere. *International Journal of Greenhouse Gas Control* 2, 388–400.
- Benson, S.M., Gasperikova, E., Hoversten, G.M., 2005. Monitoring protocols and lifecycle costs for geologic storage of carbon dioxide. *Proceedings of the 7th International Conference on Greenhouse Gas Control Technologies (GHGT-7)*, 1259–1266.
- Bergfeld, D., Evans, W.C., Howle, J.F., Farrar, C.D., 2006. Carbon dioxide emissions from vegetation-kill zones around the resurgent dome of Long Valley caldera, eastern California, USA. *Journal of Volcanology and Geothermal Research* 152, 140–156.
- Buschmann, C., Nagel, E., 1993. In vivo spectroscopy and internal optics of leaves as basis for remotes sensing of vegetation. *International Journal of Remote Sensing* 14 (4), 711–722.
- Carter, G.A., 1993. Responses of leaf spectral reflectance to plant stress. *American Journal of Botany* 80, 239–243.
- Carter, G.A., Knapp, A.K., 2001. Leaf optical properties in higher plants: linking spectral characteristics to stress and chlorophyll concentration. *American Journal of Botany* 88, 677–684.
- Carter, G.A., Miller, R.L., 1994. Early detection of plant stress by digital imaging within narrow stress-sensitive wavebands. *Remote Sensing of Environment* 50, 295–302.
- Cortis, A., Oldenburg, C.M., Benson, S.M., 2008. The role of optimality in characterizing CO₂ seepage from geologic carbon sequestration sites. *International Journal of Greenhouse Gas Control* 2, 640–652.
- Cuffey, K.M., Vimeux, F., 2001. Covariation of carbon dioxide and temperature from the Vostok ice core after deuterium-excess correction. *Nature* 412, 523–527.
- Demetriades-Shah, T.H., Steven, M.D., Clark, J.A., 1990. High resolution derivative spectra in remote sensing. *Remote Sensing of Environment* 33, 55–64.

- Gitelson, A.A., Merzlyak, M.N., 1996. Signature analysis of leaf reflectance spectra: algorithm development for remote sensing of chlorophyll. *Journal of Plant Physiology* 148, 494–500.
- Gitelson, A.A., Merzlyak, M.N., 1997. Remote estimation of chlorophyll content in higher plant leaves. *International Journal of Remote Sensing* 18, 2691–2697.
- Goetz, A.F.H., Vane, G., Solomon, J.E., Rock, B.N., 1985. Imaging spectrometry for Earth Remote Sensing. *Science* 228 (4704), 1147–1153.
- Intergovernmental Panel on Climate Change (IPCC), 2005. IPCC Special Report on Carbon Dioxide Capture and Storage. Cambridge University Press, Cambridge, UK.
- IPCC Fourth Assessment Report (AR4), 2007. IPCC Fourth Assessment Report on Climate Change. Cambridge University Press, Cambridge, UK.
- Jensen, R.R., Jackson, M.W., Lulla, V., 2008. Single line correction method to remove aircraft roll errors in hyperspectral imagery. *Journal of Applied Remote Sensing* 2, 1–10.
- Keith, C.J., Repasky, K.S., Lawrence, R.L., Jay, S.C., Carlsten, J.L., 2009. Monitoring effects of a controlled subsurface carbon dioxide release on vegetation using a hyperspectral imager. *International Journal of Greenhouse Gas Control* 3, 626–632.
- Knauss, K.G., Johnson, J.W., Steefel, C.I., 2005. Evaluation of the impact of CO₂, cocontaminant gas, aqueous fluid and reservoir rock interactions on the geologic sequestration of CO₂. *Chemical Geology* 217, 339–350.
- Knipling, E.B., 1970. Physical and physiological basis for the reflectance of visible and near-infrared radiation from vegetation. *Remote Sensing of Environment* 1 (3), 155–159.
- Korbol, R., Kaddour, A., 1995. Sleipner vest CO₂ disposal-injection of removed into the Utsira formation. *Energy Conversion and Management* 36, 509–512.
- Lawrence Berkeley National Laboratory (LBNL), 2000. An overview of geologic sequestration of CO₂. In: *ENERGEX'2000: Proceedings of the 8th International Energy Forum*, Las Vegas, NV.
- Lawrence, R.L., Labus, M., 2003. Early detection of Douglas-Fir Beetle infestation with subcanopy resolution hyperspectral imagery. *Western Journal of Applied Forestry* 18, 202–206.
- Lewicki, J.L., Hilley, G.E., Oldenburg, C.M., 2006. An Improved Strategy to Detect CO₂ Leakage for Verification of Geologic Carbon Sequestration. Lawrence Berkeley National Laboratory. <http://escholarship.org/uc/item/5cz867jk>
- Lewicki, J.L., Hilley, G.E., Dobeck, L., Spangler, L., 2010. Dynamics of CO₂ fluxes and concentrations during a shallow subsurface CO₂ release. *Environmental Earth Sciences* 60, 285–297.
- Lewicki, J.L., Oldenburg, C.M., Dobeck, L., Spangler, L., 2007. Surface CO₂ leakage during two shallow subsurface CO₂ releases. *Geophysical Research Letters* 34, <http://dx.doi.org/10.1029/2007GL032047>, L24402.
- Lillesand, T.M., Kiefer, R.W., Chipman, J.W., 2008. *Remote Sensing and Image Interpretation*, 6th Edition. John Wiley & Sons.
- Maček, I., Pfan, H., Francetić, V., Batić, F., Vodnik, D., 2005. Root respiration response to high CO₂ concentrations in plants from natural CO₂ springs. *Environmental and Experimental Botany* 54, 90–99.
- Maldal, T., Tappel, I.M., 2004. CO₂ underground storage for Snøhvit gas field development. *Energy* 29, 1403–1411.
- Male, E.J., Pickles, W.L., Silver, E.A., Hoffmann, G.D., Lewicki, J.L., Apple, M., Repasky, K., Burton, E.A., 2010. Using hyperspectral plant signatures for CO₂ leak detection during the 2008 ZERT CO₂ sequestration field experiment in Bozeman, Montana. *Environmental Earth Sciences* 60, 251–261.
- Mingzhe, D., Zhaowen, L., Shuliang, L., Huang, S., 2006. CO₂ sequestration in depleted oil and gas reservoirs-caprock characterization and storage capacity. *Energy Conservation and Management* 47, 1372–1382.
- Mokwa, R., 2006. Subsurface Exploration for the MSU CO₂ Injection Project-Phase I. Unpublished Report. Montana State University, Civil Engineering Department, 2006.
- Monnin, E., Indermühle, A., Dällenbach, A., Flückiger, J., Stauffer, B., Stocker, T.F., Raynaud, D., Barnola, J.-M., 2001. Atmospheric CO₂ concentrations over the last glacial termination. *Science* 291 (5501), 112–114.
- National Energy Technology Laboratory (NETL), 2007. Carbon Sequestration Atlas of the United States and Canada.
- National Energy Technology Laboratory (NETL), 2008. Carbon Sequestration Atlas of the United States and Canada.
- Noomen, M.F., Skidmore, A.K., 2009. The effects of high soil CO₂ concentrations on leaf reflectance of maize plants. *International Journal of Remote Sensing* 30, 481–497.
- Noomen, M.F., Smith, K.L., Colls, J.J., Steven, M.D., Skidmore, A.K., Van der Meer, F.D., 2008. Hyperspectral indices for detecting changes in canopy reflectance as a result of underground natural gas leakage. *International Journal of Remote Sensing* 29, 5987–6008.
- Oldenburg, C.M., Bryant, S.L., Nicot, J.P., 2009. Certification framework based on effective trapping for geologic carbon sequestration. *International Journal of Greenhouse Gas Control* 3, 444–457.
- Oldenburg, C.M., Lewicki, J.L., Pan, L., Dobeck, L., Spangler, L., 2010. Origin of the patchy emission pattern at ZERT CO₂ release test. *Environmental Earth Sciences* 60, 241–250.
- Petit, J.R., Jouzel, J., Raynaud, D., Barkov, N.I., Barnola, J.-M., Basile, I., Bender, M., Chappellaz, J., Davis, M., Delaygue, G., Delmotte, M., Kotlyakov, V.M., Legrand, M., Lipenkov, V.Y., Lorius, C., Pepin, L., Ritz, C., Saltzman, E., Stievenard, M., 1999. Climate and atmospheric history of the past 420,000 years from the Vostok ice core, Antarctica. *Nature* 399, 429–436.
- Pruess, K., 2008. On CO₂ fluid flow and heat transfer behavior in the subsurface, following leakage from a geologic storage reservoir. *Environmental Geology* 54, 1677–1687.
- Resonon Inc., 2008. Pika II Imaging Spectrometer. www.resonon.com/pika.html
- Rock, B.N., Hoshizaki, T., Miller, J.R., 1988. Comparison of *in situ* and airborne spectral measurements of the blue shift associated with forest decline. *Remote Sensing of Environment* 24 (1), 109–127.
- Rouse, J.H., Shaw, J.A., Lawrence, R.L., Lewicki, J.L., Dobeck, L.M., Repasky, K.S., Spangler, L.H., 2010. Multi-spectral imaging of vegetation for detecting CO₂ leaking from underground. *Environmental Earth Science* 60, 313–323.
- Rutqvist, J., Vasco, D.W., Myer, L., 2010. Coupled reservoir-geomechanical analysis of CO₂ injection and ground deformations at In Salah, Algeria. *International Journal of Greenhouse Gas Control* 4, 225–230.
- Sampson, P.H., Zarco-Tejada, P.J., Mohammed, G.H., Miller, J.R., Noland, T.L., 2003. Hyperspectral remote sensing of forest condition: estimating chlorophyll content in tolerant hardwoods. *Forest Science* 49, 381–391.
- Seigenthaler, U., Stocker, T.F., Monnin, E., Lüthi, D., Schwander, J., Stauffer, B., Raynaud, D., Barnola, J.-M., Fischer, H., Masson-Delmotte, V., Jouzel, J., 2005. Stable carbon cycle-climate relationship during the Late Pleistocene. *Science* 310, 1313–1317.
- Smith, K.L., Steven, M.D., Colls, J.J., 2004. Use of hyperspectral derivative ratios in the red-edge region to identify plant stress responses to gas leaks. *Remote Sensing of Environment* 92, 207–217.
- Smith, K.W., Vogelmann, T.C., DeLucia, E.H., Bell, D.T., Shepherd, K.A., 1997. Leaf form and photosynthesis. *BioScience* 47, 785–793.
- Spangler, L.H., Dobeck, L.M., Repasky, K.S., Nehrir, A.R., Humphries, S.D., Barr, J.L., Keith, C.J., Shaw, J.A., Rouse, J.H., Cunningham, A.B., Benson, S.M., Oldenburg, C.M., Lewicki, J.L., Wells, A.W., Diehl, J.R., Strazisar, B.R., Fessenden, J.E., Rahn, T.A., Amonette, J.E., Barr, J.L., Pickles, W.L., Jacobson, J.D., Silver, E.A., Male, E.J., Rauch, H.W., Gullickson, K.S., Trautz, R., Kharaka, Y., Birkholzer, J., Wielopolski, L., 2009. A shallow subsurface controlled release facility in Bozeman, Montana, USA, for testing near surface CO₂ detection techniques and transport models. *Environmental Earth Science*, <http://dx.doi.org/10.1007/s12665-009-0400-402>.
- Strachan, I.B., Pattey, E., Boisvert, J.B., 2002. Impact of nitrogen and environmental conditions on corn as detected by hyperspectral reflectance. *Remote Sensing of Environment* 80 (2), 213–224.
- Strazisar, B.R., Wells, A.W., Diehl, R.J., Hammack, R.W., Veloski, G.A., 2009. Near-surface monitoring for the ZERT shallow CO₂ injection project. *International Journal of Greenhouse Gas Control* 3, 736–744.
- Vogelmann, J.E., Rock, B.N., Moss, D.M., 1993. Red edge spectral measurements from sugar maple leaves. *International Journal of Remote Sensing* 14, 1563–1575.
- Whittaker, S.G., 2004. Geological storage of greenhouse gases: the IEA Weyburn CO₂ monitoring and storage project. *Canadian Society of Petroleum and Geologists Reservoir* 31 (8), 9.
- Wilson, E.J., Friedmann, S.J., Pollak, M.F., 2007. Research for deployment: Incorporating risk, regulation, and liability for carbon capture and sequestration. *Environmental Science & Technology* 41, 5945–5952.
- Xu, T., 2004. CO₂ geological sequestration. Lawrence Berkeley National Laboratory, Paper LBNL-56644 JArt.
- Zarco-Tejada, P.J., Miller, J.R., Mohammed, G.H., Noland, T.L., 2000. Chlorophyll fluorescence effects on vegetation apparent reflectance: I. Leaf-level measurements and model simulation. *Remote Sensing of Environment* 74 (3), 582–595.